Supplemental Information

S1. Setup for X-ray interface measurements

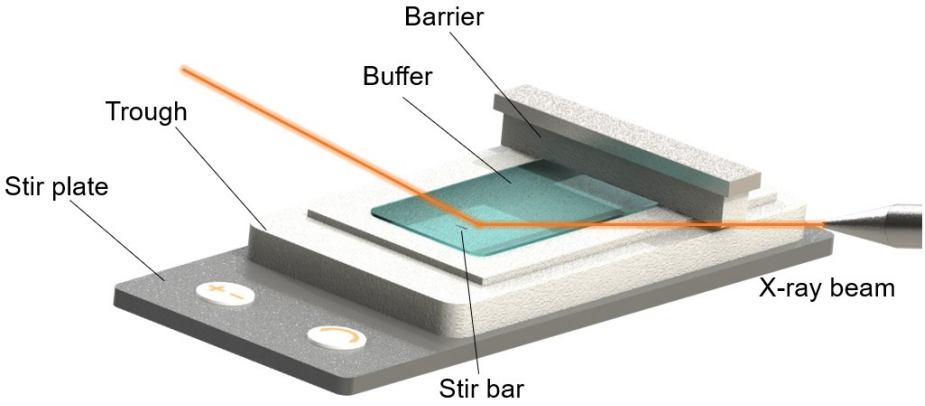

Figure s1. Schematic of integrating Langmuir trough with synchrotron X-ray beam for X-ray interface measurements.

S2. DPPC monolayers on Ca and Ca-free buffers

X-ray reflectivity and GIXD measurements of DPPC films on the Ca and Ca-free buffers were conducted at a constant surface pressure of 25 mN/m. The normalized reflectivity curves of DPPC films on both buffers were similar, as shown in **Figure s2A**. The electron density profiles (**Figure s2B**) were almost identical and both indicated monolayer interfacial structures. The two-dimensional GIXD results (**Figure s2C and D**), the Bragg peaks (**Figure s2E**) and the Bragg rods (**Figure s2F**) of DPPC on the Ca buffers were similar to those of DPPC on the Ca-free buffers, indicating similar two-dimensional lattice structures on the two buffers (**Table s1**). Therefore, Ca^{2+} alone exhibited no distinguishable effects on the interfacial organization of DPPC monolayers under our experimental conditions.

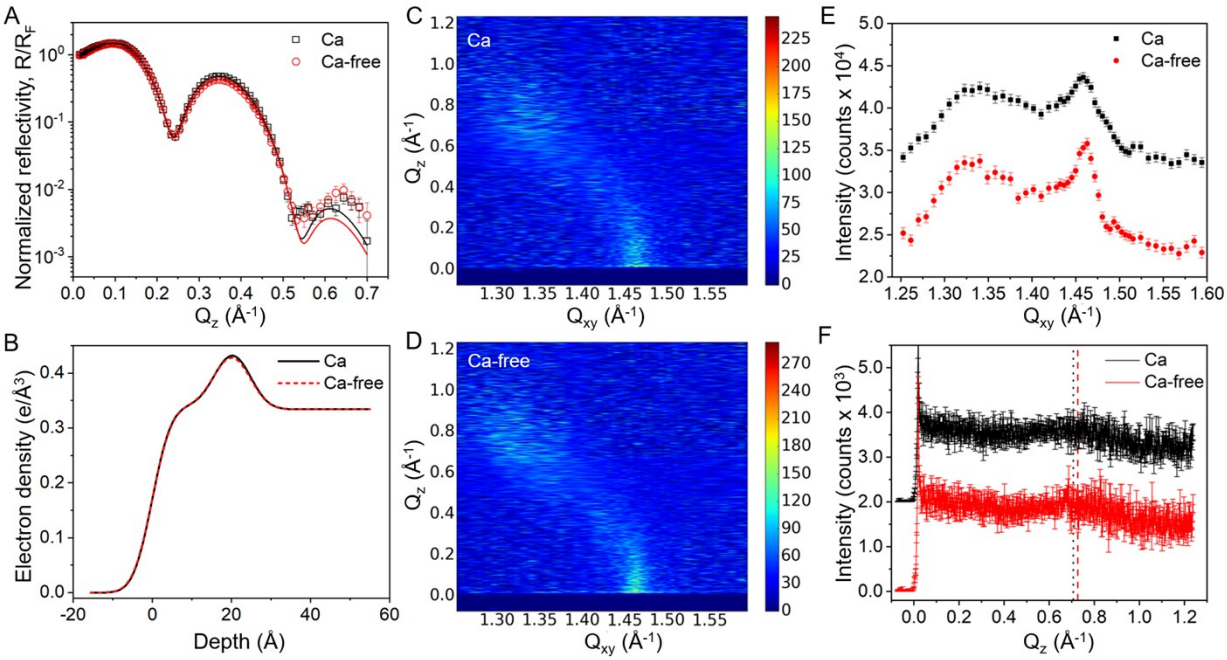

Figure s2. X-ray reflectivity and GIXD for DPPC monolayers on Ca and Ca-free buffers at constant surface pressure of 25 mN/m. (A) Normalized reflectivity of DPPC on Ca (black squares) and Ca-free (red circles) buffers. The solid lines indicate the best fits of the experimental data using single-phase box models. (B) Electron density profiles of DPPC on Ca (solid black line) and Ca-free (dotted red line) buffers. Two-dimensional GIXD results for DPPC film on (C) Ca and (D) Ca-free buffers. (E) Bragg peaks and (F) Bragg rods of DPPC films on Ca and Ca-free buffers with data offset for clarity. The vertical black dotted and red dashed line in (F) represents the peak position of the Bragg rod for the out-plane Bragg peak on the Ca and Ca-free buffer, respectively. The structural parameters are listed in **Table s1.**

Table s1. Structural parameters of DPPC on Ca and Ca-free buffers at constant surface pressure of 25 mN/m.

Parameter	Ca buffer	Ca-free buffer
σ (Å)	$3.8^{+0.1}_{-0.1}$	$3.9^{+0.1}_{-0.1}$
d_1 (Å)	$8.0^{+0.8}_{-0.5}$	$8.0^{+1.1}_{-0.5}$
ρ_1 (e/Å^3)	$0.470^{+0.007}_{-0.009}$	$0.467^{+0.005}_{-0.012}$
d_2 (Å)	$16.3^{+0.3}_{-0.6}$	$16.1^{+0.4}_{-0.6}$
ρ_2 (e/Å^3)	$0.340_{-0.003}$	$0.340_{-0.004}$
χ^2	5.4	4.5
Azimuth of tilt	NN tilt	NN tilt
$Q_{xy[1,1]}$, Å^{-1}	$1.336^{\pm 0.005}$	$1.332^{\pm 0.004}$
$Q_{xy[0,2]}$, Å^{-1}	$1.459^{\pm 0.001}$	$1.460^{\pm 0.001}$
$Q_{z[1,1]}$, Å^{-1}	$0.708^{\pm 0.006}$	$0.727^{\pm 0.005}$
Area per molecule, Å^2	$48.4^{\pm 0.4}$	$48.4^{\pm 0.4}$
Tilt angle, ^{o}	$32.2^{\pm 0.3}$	$33.1^{\pm 0.4}$

The electron density of the aqueous phase was 0.334 e/Å^3. The first slab (labelled 1) represents the head group region, and the second slab is for the tail region. The error bar for each parameter was calculated based on one

S3. Pressure-area change during X-ray measurements.

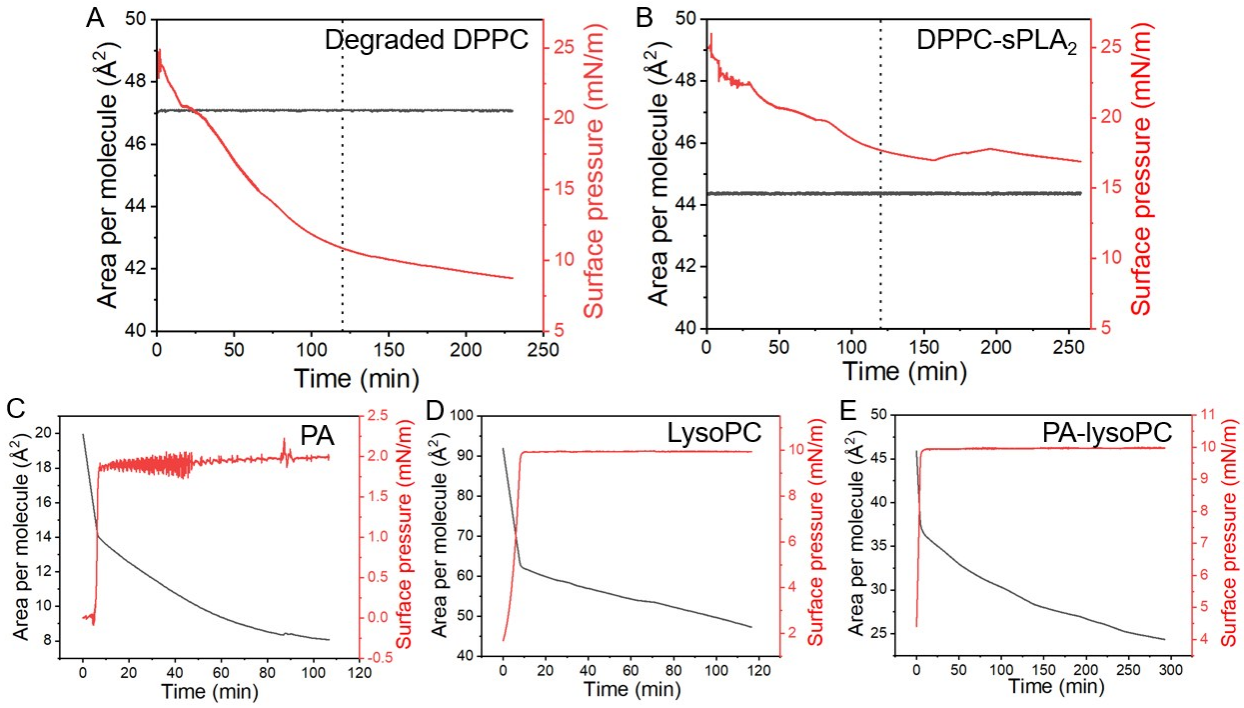

Figure s3. Pressure and area change during X-ray measurements. (A) For DPPC film, the area was set constant and $sPLA_2$ was added to the subphase Ca buffer at the original time point. The interfacial pressure decreased from 25 mN/m to about 10 mN/m. Dotted lines represent 120 minutes after enzyme injection, when X-ray measurements were initiated for the degraded DPPC film. (B) For DPPC film, the area was set constant and $sPLA_2$ added to the subphase Ca-free buffer at the original time point. The dotted lines represent 120 minutes after enzyme injection, when X-ray measurements were initiated for the DPPC-$sPLA_2$ film. (C) For PA film on Ca buffer the pressure was set constant at 2 mN/m. The area reduced with time. (D) For lysoPC on Ca buffer the pressure was set constant at 10 mN/m. The area reduced with time. (E) For the film of PA-lysoPC equimolar mixture on Ca buffer the pressure was set constant at 10 mN/m. The area per molecule for the mixture was obtained using the surface area divided by the total molecular number of the mixture. The area reduced with time. For PA, lysoPC and PA-lysoPC films, X-ray measurements were started immediately after the target pressures were reached.

S4. X-ray reflectivity for PA film on Ca buffer at 10 mN/m

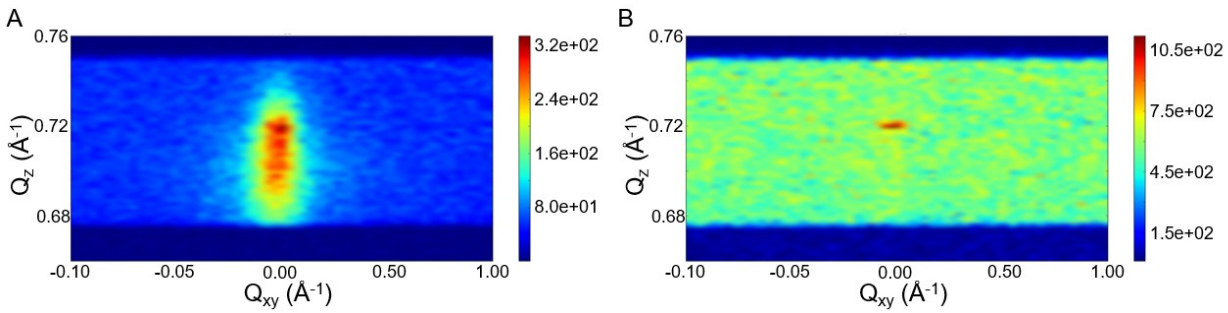

Figure s4. Recorded intensity of X-ray reflectivity at vertical momentum vector Q_z = 0.72 Å^{-1} for PA film on different buffers at constant pressure of 10 mN/m. (A) Ca buffer and (B) Ca-free buffer.

S5. PA films on Ca-free buffer

A single-phase three-box model was used to best fit the normalized reflectivity data for the PA film on the Ca-free buffer at 2 mN/m and 10 mN/m. The additional layer might have been the accumulated tris molecules under the head region of deprotonated carboxyl groups of PA molecules. The normalized reflectivity curves and the electron density profiles (**Figure s5A**) indicated a monolayer interfacial structure. The GIXD Bragg peaks for the PA film on the Ca-free buffer at the surface pressures of 2 and 10 mN/m (**Figure s5B**) showed an out-plane peak at a lower Q_{xy} position and an in-plane peak at a higher Q_{xy} position, indicating NN-tilted packing structure. The obtained structural parameters are listed in **Table s2**.

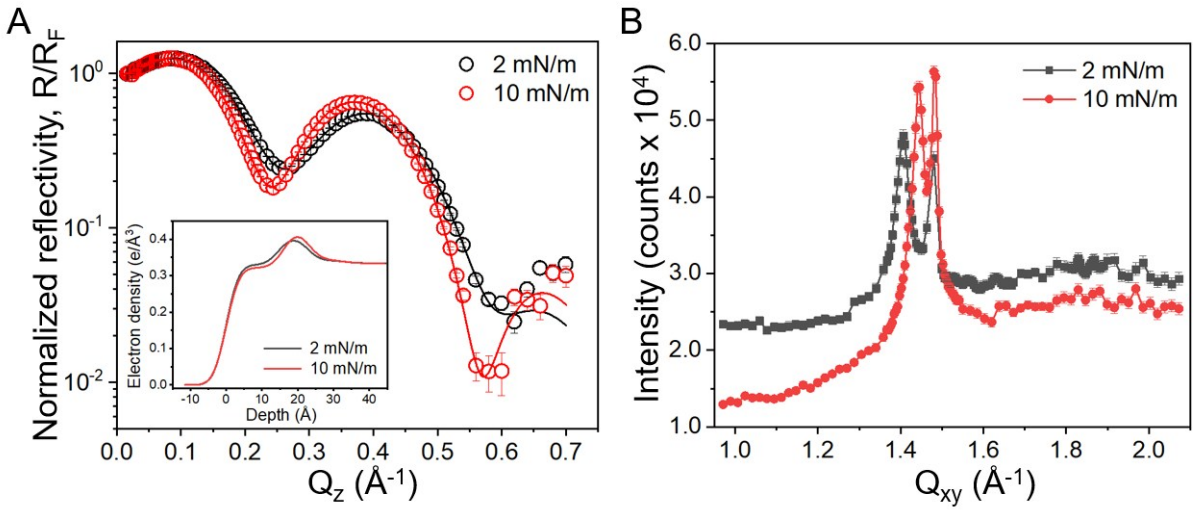

Figure s5. X-ray reflectivity and GIXD for PA films on Ca-free buffer at constant pressures of 2 mN/m and 10 mN/m. (A) Normalized X-ray reflectivity. Symbols are the experimental data, and solid lines

represent the corresponding best fit of the data using the single-phase box model. Electron density profiles are in the inset. (B) GIXD Bragg peaks. The structural parameters are listed in **Table s2**.

Table s2. Structural parameters of PA films on Ca-free buffer at constant pressures of 2 mN/m and 10 mN/m.

Subphase	Ca-free buffer	Ca-free buffer
Surface pressure (mN/m)	2	10
σ (Å)	$2.8^{+0.2}_{-0.1}$	$2.9^{+0.1}_{-0.2}$
d_1 (Å)	$10.8^{+1.5}_{-0.2}$	$9.6^{+0.5}_{-0.7}$
ρ_1 (e/Å^3)	$0.341^{+0.001}_{-0.003}$	$0.343^{+0.001}_{-0.002}$
d_2 (Å)	$8.0^{+1.1}_{-0.1}$	$6.9^{+0.9}_{-0.8}$
ρ_2(e/Å^3)	$0.407^{+0.001}_{-0.007}$	$0.427^{+0.007}_{-0.010}$
d_3 (Å)	$14.7^{+0.1}_{-0.8}$	$16.2^{+0.1}_{-0.6}$
ρ_3 (e/Å^3)	$0.330^{+0.005}_{-0.004}$	$0.321^{+0.002}_{-0.003}$
χ^2	10.0	3.3
$Q_{xy\,[1,1]}$ (Å^{-1})	$1.406^{\pm 0.001}$	$1.444^{\pm 0.001}$
$Q_{xy\,[0,2]}$ (Å^{-1})	$1.476^{\pm 0.001}$	$1.484^{\pm 0.001}$
$Q_{z[1,1]}$ (Å^{-1})	$0.553^{\pm 0.005}$	$0.440^{\pm 0.005}$
Area per tail (Å^2)	$22.3^{\pm 0.1}$	$21.5^{\pm 0.1}$
Tilt angle (^{o})	$24.8^{\pm 0.2}$	$19.6^{\pm 0.3}$

S6. Second-order GIXD peak of organized Ca^{2+} layer

When the Q_{xy} range of GIXD measurement was increased to 2.2 $Å^{-1}$, we detected an additional GIXD peaks at 2.151 $Å^{-1}$ for the PA on Ca buffer at a constant pressure of 2 mN/m and at 2.147 $Å^{-1}$ for the degraded DPPC film. Their Bragg peaks and Bragg rods are presented in **Figure s6**. The intensities of both Bragg rods remained almost constant for the entire Q_z range. The slow intensity decay was similar to the GIXD peaks at 1.075 $Å^{-1}$, which indicated that these peaks were scattered from a thin Ca^{2+} layer. Furthermore, the GIXD peak position at about 2.15 $Å^{-1}$ was about twice the Q_{xy} of the first-order Ca^{2+} peaks at 1.075 $Å^{-1}$ (**Figure 3A**). Therefore, GIXD peaks at about 2.15 $Å^{-1}$ were likely the second-order peaks of the GIXD peak at 1.075 $Å^{-1}$ scattered from the organized Ca^{2+} layer.

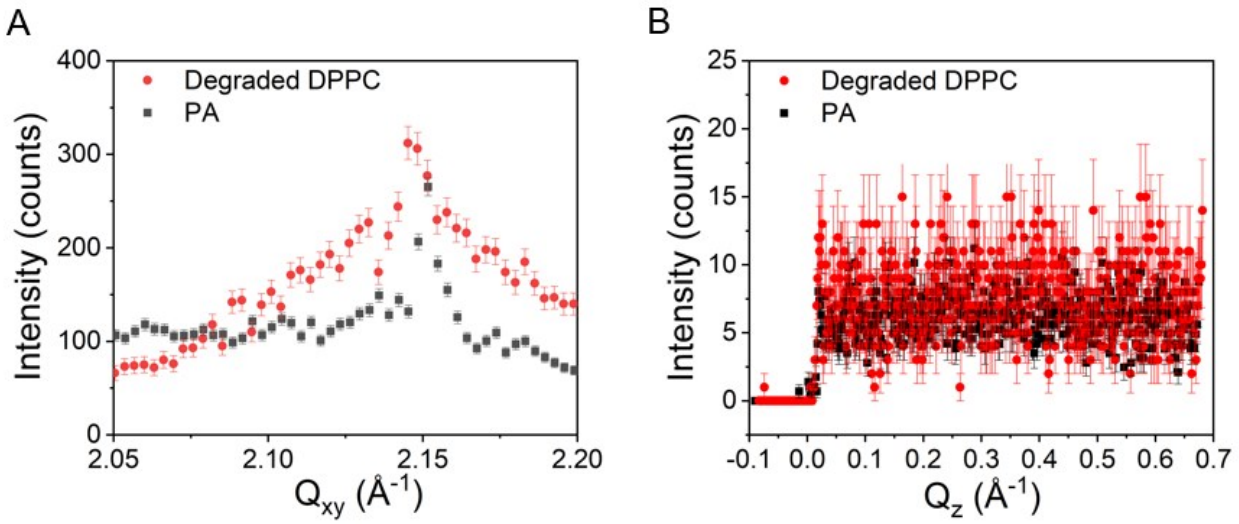

Figure s6. Second-order GIXD peak scattered from the organized Ca^{2+} layer. (A) Bragg peaks in Q_{xy} range from 2.05 Å to 2.2 Å and (B) their corresponding Bragg rods for degraded DPPC film and PA film on Ca buffer. GIXD intensities of the PA films are reduced by half for comparison.

S7. Phase distribution of PA-lysoPC film on Ca buffer

The phase distribution of PA-lysoPC films on the Ca buffer at the gas-liquid interface was measured using a trough (51 x 155 mm^2) mounted on an inverted fluorescence microscope (Observer D1-AX10, Zeiss). Lipids were dissolved in chloroform and stored at -20°C. For each sample, 1 mol% 1,2-dipalmitoyl-sn-glycero-3-phosphoethanolamine-N- (lissamine rhodamine B sulfonyl) (DPPE-Rhod) was added to provide contrast. The trough was cleaned and filled with 53 mL Ca buffer as the subphase. The cleanliness of the surface was checked, and the lipid sample was spread on the subphase using the method described in the **Experimental** section in the text. The monolayer was then compressed by two symmetric barriers at a total speed of 6 mm/min until the target pressure of 10 mN/m was reached, and then the film was maintained at this pressure. The temperature of the subphase was monitored by a built-in

thermocouple inserted within the aqueous phase and was maintained at 23±0.5°C by a water circulation system (Anova Scientific). The interfacial tension was measured by a platinum Wilhelmy plate attached to an electronic balance. The fluorescence microscope was equipped with a 20x objective (LD Plan-NEOFLUAR, Zeiss), and the fluorescent light of the inverted fluorescence microscope was provided by an X-Cite series 120 Q bulb with a TEXAS RED filter set (Ex/Em 565 nm/620 nm).

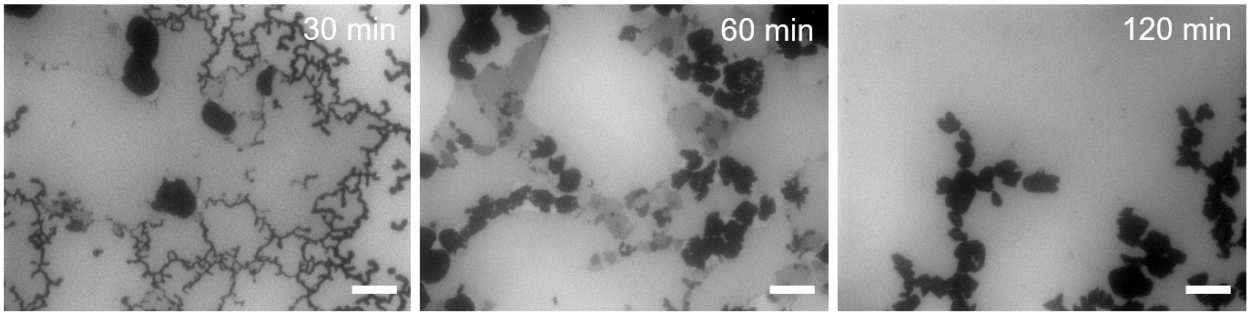

Figure s7. Representative phase distribution of PA-lysoPC films after reaching 10 mN/m for 30, 60, and 120 minutes on Ca buffer. The scale bar in each frame represents 50 μm.

As shown in **Figure s7**, when the PA-lysoPC film was maintained at the surface pressure of 10 mN/m, multiple phases were coexisted at the interface. The interface was mainly covered by a bright surrounding phase with an average surface coverage of about 80%, and the rest was covered by a combination of dark networks and domains. Because the fluorescent dye, DPPE-Rod, preferred the liquid phase over the gel phase, the bright surrounding phase was likely composed of mainly lysoPC molecules, which were in the liquid phase under our experimental conditions. On the other hand, the dark networks and round domains were likely composed of mainly PA molecules.